Analysis of Three-Dimensional Unsteady Viscous Flow around Oscillating Wings

THEODORE BRATANOW* AND AKIN ECER†
University of Wisconsin-Milwaukee, Milwaukee, Wis.

A method based on the Navier-Stokes equations was applied for analyzing the three-dimensional unsteady flow around oscillating wings. These equations were treated in the complete three-dimensional form considering also the irregular geometry of the wing. The vorticity transport equations were discretized using three-dimensional finite elements from a variational formulation and integrated numerically. At each time step of the numerical integration, the velocity field was determined from a representation of the three-dimensional wing by a system of optimized distribution of discrete vortices superimposed on the flow space. The time-dependent boundary conditions on the oscillating wing were specified as external constraint conditions at each step of the numerical integration. Examples of obtained results describing the three-dimensional unsteady flow around a wing were presented.

Nomenclature

$\mathbf{A}$ = vector representing the approximation functions for the finite element discretization
$\mathbf{a}$ = a Boolean matrix for the assembly of element matrices in a global form
B = span length of the wing, in m
b_i = imposed constraints representing the boundary conditions around the wing
$\mathbf{b}_\omega$ = matrix formulation of boundary conditions represented by b_i
C = chord length of the wing, in m
$\mathbf{C}$ = vector representing the induced velocities at several points on the wing surface by the surrounding vorticity field
$\mathbf{e}_{\omega j}$ = vector [see Eq. (17)]
$\mathbf{h}_{\omega j}$ = vector [see Eq. (16)]
N = number of finite elements on one side of the cubic grid-work in Fig. 1
p = pressure, lbf/in.^{2} (N/m^2)
$\mathbf{P}$ = matrix derived from Eq. (31) describing the effect of a point vortex or doublet at a point on the wing
$\mathbf{q}_{\omega j}$ = vector [see Eq. (19)]
$\mathbf{p}, \mathbf{q}, \mathbf{r}$ = global velocity vectors which consist of the nodal velocities of the finite element gridwork in each of the x, y, z directions
$\mathbf{r}$ = vector representing the relative position of a point on the wing surface with respect to the surrounding vorticity field
$\mathbf{r}^*$ = vector representing the relative position of a point on the wing surface with respect to a point vortex representing the wing
$\mathbf{r}_\omega$ = matrix [see Eq. (20)]
S = surface area of the wing, in.^{2} (m^2)
$\mathbf{S}$ = diagonal matrix assembled from the areas of surface elements on the wing
$\mathbf{S}_\omega$ = a square matrix describing the coupling between nodal values of vorticities
$\mathbf{S}_\omega{}^e$ = element matrix for the coupling between nodal values of vorticities
$\mathbf{T}_c$ = finite element matrix describing the convection terms
$\mathbf{T}_d$ = finite element matrix describing the coupling between the vorticities in x, y, z directions
$\mathbf{T}_v$ = finite element matrix describing the viscous terms
$\mathbf{U}$ = global velocity vector including the components of velocities in x, y, z directions [see Eq. (14)]
$\mathbf{u}$ = vector representing the velocity field in three-dimensional space $\mathbf{u} = [u_1 u_2 u_3]$, in./sec (m/sec)
u_i = the magnitude of the velocity vector at ith point on the wing surface, in./sec (m/sec)
u_n = normal velocity at the surface of the wing, in./sec (m/sec)
V = volume of a finite element, in.^{3} (m^3)
$\mathbf{W}_j$ = vorticity vector which consists of the jth component of vorticities at each node
$d\mathbf{W}_j/dt$ = vector which consists of time derivatives of the jth component of vorticities at each node
X, Y, Z = coordinates of points on the wing surface, in. (m)
x, y, z = rectangular coordinates, in. (m)
x_i, y_i, z_i = coordinates of a point vortex, in. (m)
Γ = a quadratic function [see Eq. (29)]
$\tilde{\Gamma}$ = discrete approximation of Γ at m points on the wing surface
γ = vector representing the magnitude of point vorticities describing the wing
δ = vector representing the Lagrangian multipliers
Δt = incremental time step, sec
ζ, η, ξ = nondimensional coordinate system for a finite element
ν = kinematic viscosity, in.^{2}/sec (m^2/sec)
Ξ = nondimensionalized error function [see Eq. (38)]
Ξ^* = nondimensional error function for optimization [see Eq. (39)]
ρ = mass density, lbm/in.^{3} (kg/m^3)
Φ = variational functional in the finite element formulation
$\tilde{\Phi}$ = the variational functional including the boundary conditions
χ = a matrix [see Eq. (27)]
$\boldsymbol{\omega}$ = vector representing the vorticity field in three-dimensional space $\boldsymbol{\omega} = [\omega_1 \omega_2 \omega_3]$, 1/sec
∇ = del operator $\nabla = (\partial/\partial x)\mathbf{i} + (\partial/\partial y)\mathbf{j} + (\partial/\partial z)\mathbf{k}$
∇^2 = Laplace operator $\nabla^2 = \partial^2/\partial x^2 + \partial^2/\partial y^2 + \partial^2/\partial z^2$

Subscripts
0 = at time $t = 0$
x, y, z = derivatives with respect to x, y, z

I. Introduction

IN unsteady aerodynamics the Navier-Stokes equations can be applied for analysis of unsteady flow around irregularly shaped oscillating obstacles. The numerical solution of these equations in three-dimensional space becomes intractable particularly because of the size of the discretized system of differential equations to be solved for obtaining accurate results. Even for two-dimensional flow problems, numerical solutions have been in general restricted to simplified cases,[1,2] and a direct application of these methods to three-dimensional flow problems does not appear as practical with present computers. Examples of numerical solutions of three-dimensional flow problems exist for

Presented as Paper 74-184 at the AIAA 12th Aerospace Sciences Meeting, Washington, D.C., January 30–February 1, 1974; submitted April 19, 1974; revision received June 13, 1974. This research was supported by NASA under Grant NGR-50-007-001.
Index category: Nonsteady Aerodynamics.
* Professor of Engineering Mechanics. Member AIAA.
† Assistant Professor of Engineering Mechanics. Member AIAA.

axisymmetric cases,[3,4] and again for simple obstacle geometric configurations. Other investigators were able to treat a specific portion of the general phenomenon, as described by the complete set of Navier-Stokes equations.[5]

The authors have previously applied the finite element method for solution of the Navier-Stokes equations in two-dimensional space.[6-8] In this paper an application of the same method is presented for the analysis of three-dimensional unsteady incompressible flow around an oscillating wing. The method is capable of treating the complete form of the Navier-Stokes equations for arbitrary wing geometric configurations undergoing an arbitrary motion. After the presentation of the mathematical model in a general form, each phase of the analysis is discussed in detail in relation to computer storage and computer time. One of the advantages of this formulation is the ability in treating each of the terms in the equations separately and combining them in an efficient manner. Compared to finite-difference techniques, where a single finite-difference molecule describes the entire system, this approach becomes advantageous in streamlining the calculations during the solution of the discrete system of equations.[7] The numerical method establishes a capability of treating three-dimensional flow problems in a most general manner, using present-day computers, without making any restrictive assumptions in the actual three-dimensional characteristics of the unsteady flow.

For this investigation it was convenient to analyze the unsteady flow at high Reynolds numbers mainly in terms of the distribution of vorticity. The mathematical formulation involves a discrete variational formulation of the vorticity transport equations in terms of the vorticity and velocity distributions around the oscillating wing. The Lagrangian multiplier technique was applied for representing the time-dependent boundary conditions corresponding to the instantaneous positions and motion of the wing. The instantaneous velocity field was determined at each time step by using a generalized form of the method of singularities.

II. Mathematical Background

The vorticity transport equations can be written in three-dimensional space as

$$\partial\boldsymbol{\omega}/\partial t+(\mathbf{u}\cdot\nabla)\boldsymbol{\omega}=(\boldsymbol{\omega}\cdot\nabla)\mathbf{u}+\nu\nabla^2\boldsymbol{\omega} \tag{1}$$

where $\boldsymbol{\omega}$ is the vorticity vector. The velocity field is related to the vorticity field as

$$\nabla\times\mathbf{u}=\boldsymbol{\omega} \tag{2}$$

The velocity field $\mathbf{u}$ must also satisfy the condition of incompressibility

$$\nabla\cdot\mathbf{u}=0 \tag{3}$$

The pressure distribution corresponding to the instantaneous velocity field can be calculated from a supplementary equation

$$\nabla^2 p=-2\rho\left(\frac{\partial U_2}{\partial X}\frac{\partial U_1}{\partial Y}+\frac{\partial U_3}{\partial X}\frac{\partial U_1}{\partial Z}+\frac{\partial U_3}{\partial Y}\frac{\partial U_2}{\partial Z}-\frac{\partial U_1}{\partial X}\frac{\partial U_2}{\partial Y}-\frac{\partial U_1}{\partial X}\frac{\partial U_3}{\partial Z}-\frac{\partial U_2}{\partial Y}\frac{\partial U_3}{\partial Z}\right) \tag{4}$$

The analysis of unsteady incompressible flow requires the numerical integration of Eq. (1) while at each time step the instantaneous velocity field is determined from the simultaneous solution of Eqs. (2) and (3). The pressure distribution can be calculated at desired time instances from the solution of Eq. (4). In the following, the application of the finite element method for the numerical integration of vorticity transport equations in three-dimensional space will be discussed first. Then the application of the method of singularities for the solution of Eqs. (2–4) will be described.

III. Numerical Integration of the Vorticity Transport Equations

The finite element method was applied for the numerical integration of the vorticity transport equation in two-dimensional space by the authors and others.[5-10] This method can be applied for the solution of three-dimensional problems in the following manner.

A. Variational Formulation

The solution of Eq. (1) can be obtained by minimizing the following variational functional

$$\Phi=\int_V\omega_i\frac{\partial\omega_i}{\partial t}dV+\frac{1}{2}\int_V\omega_i u_j\frac{\partial\omega_i}{\partial x_j}dV+\frac{\nu}{2}\int_V\left(\frac{\partial\omega_i}{\partial x_j}\right)^2dV-\frac{1}{2}\int_V\omega_i\omega_j\frac{\partial u_i}{\partial x_j}dV \tag{5}$$

where $(\omega_i, i=1,3)$ are the vorticities and $(u_j, j=1,3)$ are the velocities in x,y,z directions. The nonlinear terms in the variational functional can be calculated from a series expansion of the instantaneous velocities due to incremental changes in the vorticities as

$$u_i=u_i\Big|_0+\frac{\partial u_i}{\partial\omega_j}\Big|_0\Delta\omega_j+\frac{1}{2}\frac{\partial^2 u_i}{\partial\omega_j\partial\omega_k}\Big|_0\Delta\omega_j\Delta\omega_k+\cdots \tag{6}$$

Each of the terms in the series in Eq. (6) can be calculated directly by determining the incremental changes of velocity at a certain point induced by an incremental change in the vorticity at another point.[11] In determining u_i which satisfies Eqs. (2) and (3), a new numerical procedure for the three-dimensional case was developed. The variational functional in Eq. (5) converges to the exact variational form from the series approximation of Eq. (6).

The finite element method can be applied to discretize both Eqs. (5) and (6) and obtain a system of discrete equations. A set of differential equations are thus obtained by minimizing the variational functional with respect to discrete values of vorticities at the nodes of a finite element gridwork.

B. Finite Element Discretization

The vorticity field in three-dimensional space can be discretized by finite elements as

$$\omega_j(x,y,z)=A^i(x,y,z)w_j^i \tag{7}$$

where w_j^i is the jth component of the vorticities at the ith node of a finite element and A^i is the approximation function for the element. The element vorticity vector $\mathbf{w}$ is related to a global vorticity $\mathbf{W}$ by a linear relationship

$$\mathbf{W}_j=\sum_g\mathbf{a}^i\mathbf{w}_j^i \tag{8}$$

where the summation over g represents the assembly of the finite elements.

By substituting Eqs. (7) and (8) into Eq. (5) a discrete variational functional can be obtained in terms of the nodal vorticities of the finite element gridwork. By minimizing the resulting discrete variational functional with respect to W_j^i a system of first-order nonlinear ordinary differential equations is obtained as

$$\mathbf{S}_\omega(d\mathbf{W}_j/dt)=-[\mathbf{T}_c(\mathbf{U})+\mathbf{T}_v]\mathbf{W}_j+\mathbf{T}_d{}^j(\mathbf{W}_k) \tag{9}$$

where

$$\mathbf{S}_\omega=\sum_g\int_V\mathbf{A}^t\mathbf{A}\,dV \tag{10}$$

$$\mathbf{T}_v=\sum_g\int_V\nu[\mathbf{A}_x{}^t\mathbf{A}_x+\mathbf{A}_y{}^t\mathbf{A}_y+\mathbf{A}_z{}^t\mathbf{A}_z]\,dV \tag{11}$$

$$\mathbf{T}_c(\mathbf{U})=\sum_g\int_V[\mathbf{A}^t\mathbf{A}(\mathbf{p}\mathbf{A}_x+\mathbf{q}\mathbf{A}_y+\mathbf{r}\mathbf{A}_z)]\,dV \tag{12}$$

$$\mathbf{T}_d{}^1(\mathbf{W}_k)=\sum_g\int_V\{\mathbf{A}^t[\mathbf{A}_x\mathbf{p}\mathbf{A}\mathbf{W}_1+\mathbf{A}_y\mathbf{p}\mathbf{A}\mathbf{W}_2+\mathbf{A}_z\mathbf{p}\mathbf{A}\mathbf{W}_3]\}\,dV \tag{13}$$

etc. Matrices $\mathbf{T}_v$ and $\mathbf{T}_c$ represent the viscous and convective terms, respectively, in Eq. (1). $\mathbf{T}_c$ contains nonlinearities due to

the velocity terms, which can be treated using the discrete formulation of Eq. (6) as

$$\mathbf{U}|_{\Delta t} = \begin{bmatrix} \mathbf{p} \\ \mathbf{q} \\ \mathbf{r} \end{bmatrix}_{\Delta t} = \mathbf{U}_0 + \frac{\partial \mathbf{U}}{\partial w_j^i}\bigg|_0 \Delta w_j^i + \frac{1}{2}\frac{\partial^2 \mathbf{U}}{\partial w_j^i \partial w_1^k}\bigg|_0 \Delta w_j^i \Delta w_1^k + \cdots \tag{14}$$

The vector $\mathbf{U}_0$ and its derivatives at a particular instance can be calculated as the induced incremental velocity at a point ΔU_i due to an incremental increase in the vorticity field at another point, Δw_j^i, which satisfies Eqs. (2) and (3). The elements of **p**, **q**, and **r** vectors consist of the velocities at each node of the finite element gridwork in x, y, z directions, respectively. Matrix $\mathbf{T}_d$ represents the coupling between vorticities due to the velocity terms.

C. Boundary Conditions

The system of equations shown in Eq. (9) does not include the boundary conditions in three-dimensional space at the surface of the wing. Instead of modifying the system of equations for instantaneous positions and motion of the wing, one can superimpose the wing boundary conditions as external constraints. This can be done using the Lagrangian multiplier technique[12] as follows.

The variational formulation of Eq. (1) shown in Eq. (5) was modified to include the wing boundary conditions by adding the boundary conditions as a series of constraints on the variational functional. The minimum of the following function

$$\tilde{\Phi} = \Phi + b_i \delta_i \tag{15}$$

satisfies these boundary conditions, where the $b_i \delta_i$ are a linear system of constraints describing the boundary conditions at a series of points on the wing surface. The δ_i are the Lagrangian multipliers corresponding to each of these boundary conditions. By minimizing Eq. (15), a system of first-order partial differential equations is obtained as follows:

$$\begin{bmatrix} \mathbf{S}_\omega & \mathbf{b}_\omega \\ \mathbf{b}_\omega^t & \mathbf{0} \end{bmatrix} \begin{bmatrix} d\mathbf{W}_j/dt \\ \boldsymbol{\delta} \end{bmatrix} = \begin{bmatrix} \mathbf{h}_{\omega j} \\ \mathbf{e}_{\omega j} \end{bmatrix} \tag{16}$$

where the boundary conditions around the wing are

$$\mathbf{b}_\omega^t (d\mathbf{W}_j/dt) = \mathbf{e}_{\omega j} \tag{17}$$

Each column of $\mathbf{b}_\omega$ and corresponding term $\mathbf{e}_{\omega j}$ describe the rate of vorticity $\partial \omega_j/\partial t$ at a boundary point on the wing surface in terms of the elements of vector $d\mathbf{W}_j/dt$. The vector $d\mathbf{W}_j/dt$ is calculated for instantaneous vorticity and velocity distributions from Eq. (16). The efficiency of the above formulation in the solution of three-dimensional flow problems is described in the following section.

D. Solution of the Discretized Equations

The solution of Eq. (16) can be written as

$$d\mathbf{W}_j/dt = \mathbf{q}_{\omega j} - \mathbf{r}_\omega (\mathbf{b}^t \mathbf{r}_\omega)^{-1} (\mathbf{b}_\omega{}^t \mathbf{q}_{\omega j} - \mathbf{e}_{\omega j}) \tag{18}$$

where

$$\mathbf{q}_{\omega j} = \mathbf{S}_\omega{}^{-1} \mathbf{h}_{\omega j} \tag{19}$$

and

$$\mathbf{r}_\omega = \mathbf{S}_\omega{}^{-1} \mathbf{b}_\omega \tag{20}$$

The matrix $\mathbf{S}_\omega$ represents the flowfield without the obstacle and it does not change as the wing moves. In the special case of a stationary wing, only the $\mathbf{e}_{\omega j}$ and $\mathbf{h}_{\omega j}$ and therefore the $\mathbf{q}_{\omega j}$ change, while the $\mathbf{b}_\omega$ and $\mathbf{r}_\omega$ remain the same.

The major computational difficulty in the solution of Eq. (18) is the implementation of the inversion of the matrix $\mathbf{S}_\omega$ in Eqs. (19) and (20). For the accurate representation of the wing geometry in matrix $\mathbf{b}_\omega$, the order of matrices $\mathbf{b}_\omega$ and $\mathbf{r}_\omega$ becomes too large in terms of both computer storage and computation time. Although the developed method remains general, as far as the choice of the finite-element gridwork is concerned, a uniform gridwork as shown in Fig. 1 was chosen in treating the above

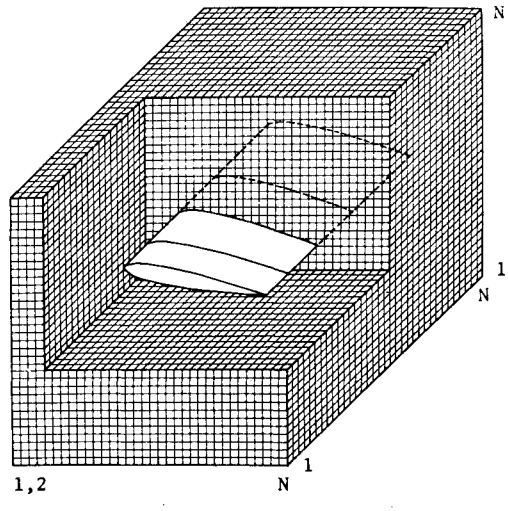

Fig. 1 Three-dimensional finite element gridwork.

computational difficulties. Each of the elements of the finite element gridwork is a cube. In this case, the inverse of matrix $\mathbf{S}_\omega$ can be obtained in a closed form for an element in the freestream. The details of the derivation of the finite element model are described in Sec. III-E.

E. Finite Element Model

A typical finite element used in the discrete representation of the flowfield is shown in Fig. 2. In this case, assuming a linear variation of vorticities over each element, vector $\mathbf{A}^j$ in Eq. (7) can be written as

$$A_i{}^j(x, y, z) = \tfrac{1}{8}(1+\zeta\zeta_i)(1+\eta\eta_i)(1+\xi\xi_i) \tag{21}$$

where the nondimensionalized coordinates ζ, η, ξ are defined as

$$\zeta = \left[x - \frac{x_2+x_4}{2}\right] \Big/ \left(\frac{x_4-x_2}{2}\right) \tag{22}$$

$$\eta = \left[y - \frac{y_2+y_4}{2}\right] \Big/ \left(\frac{y_4-y_2}{2}\right) \tag{23}$$

$$\xi = \left[z - \frac{z_5+z_1}{2}\right] \Big/ \left(\frac{z_1-z_5}{2}\right) \tag{24}$$

and ζ_i, η_i, and ξ_i are the coordinates of the nodes of the cube.

Each of the terms in Eq. (9) can then be defined by substituting Eq. (21) in Eqs. (10–12) and integrating the resulting expressions over the volume of each finite element. The advantage of choosing a uniform gridwork, with identical elements, is that the element matrices are the same for every element.

Matrix $\mathbf{S}_\omega$ in Eq. (9) becomes

$$\mathbf{S}_\omega = \sum_g \mathbf{S}_\omega{}^{ei} \tag{25}$$

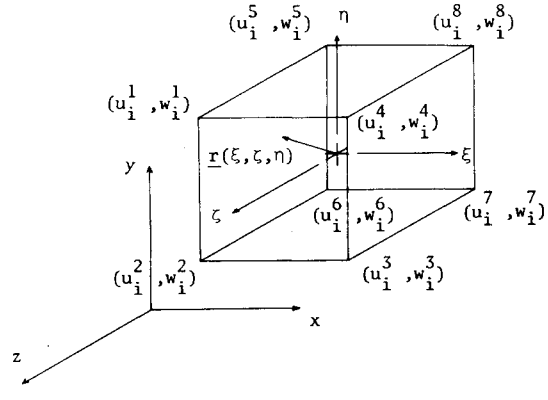

Fig. 2 Typical three-dimensional finite element used in the analysis.

where

$$\mathbf{S}_\omega{}^e = \frac{V}{27}\begin{bmatrix} 2\psi & \psi \\ \psi & 2\psi \end{bmatrix} \tag{26}$$

$$\psi = \begin{bmatrix} 4 & 2 & 1 & 2 \\ 2 & 4 & 2 & 1 \\ 1 & 2 & 4 & 2 \\ 2 & 1 & 2 & 4 \end{bmatrix} \tag{27}$$

and V is the volume of the finite element. Considering a three-dimensional space of $N \times N \times N$ finite elements, the size of matrix $\mathbf{S}_\omega$ increases quite rapidly with N. Therefore, even if the inverse of matrix $\mathbf{S}_\omega$ can be calculated economically as in the case of Eq. (25), the use of all the terms in the inverse matrix in the numerical integration becomes an extravagant computational effort. At this point a further simplification can be made in the finite element gridwork, and the inverse of the matrix is calculated only for the nodes at the neighborhood of the wing where the viscous effects are important. The coupling effects between nodes farther away from each other than a reasonable distance can also be neglected. As a result of such simplification, the size of matrix $\mathbf{r}_\omega$ is reduced considerably.[20]

The inverse of matrix $\mathbf{S}_\omega$ is obtained with a recurrence relationship, whereby each element of the matrix can be computed directly. In this manner matrix $\mathbf{S}_\omega$ does not have to be stored. Only the matrices $\mathbf{r}_\omega$ and $\mathbf{q}_{\omega j}$ have to be calculated and stored, which reduces the computational effort considerably.

The computation of vector $\mathbf{h}_{\omega j}$, which includes the viscous and convective terms, also requires an extensive computational effort. The viscous and convective effects induced at every point of the finite element gridwork have to be calculated in terms of the entire vorticity field. Although there was no storage space problem involved, the computer time became excessive with increasing number of nodes in the finite element gridwork. Therefore, vector $\mathbf{h}_{\omega j}$ was calculated only for elements in a region around the wing.[20] Further simplification in the calculation of viscous and convective terms was made following a similar arrangement of matrix $\mathbf{r}_\omega$.

As can be seen from Eq. (12), in three-dimensional space the convective terms are coupled only in terms of velocities. The procedure is repeated for the vorticities in x, y, and z directions, respectively, using the same matrix $\mathbf{S}_\omega$. The determination of the velocity field at each time step of the numerical integration is described in Sec. IV.

IV. Determination of the Velocity Field

For the two-dimensional finite element analysis of incompressible flow, a stream function-vorticity formulation was applied.[6] In the solution of the resulting Poisson's equation the unknowns were the velocities at each point of the finite element gridwork. In three-dimensional space a direct solution of Eqs. (2) and (3) would be uneconomical. For an accurate representation of the three-dimensional wing problem, the number of equations from which velocities are calculated increases very rapidly with the number of grid points. Therefore, in this paper the method of singularities was applied for determining the velocity field around the oscillating wing from Eq. (14).

A. Method of Singularities

Von Kármán used the method of singularities in analyzing potential flow around obstacles by representing the obstacle as a series of point vortices. However, for arbitrary obstacle shapes the problem becomes strongly dependent on the position of these point vortices. Prager's method in treating the problem was to represent the obstacle by a surface vorticity distribution over the obstacle.[13] With the advancement of computers, this approach has been widely applied in aerodynamics during recent years. Hess and Smith[14] have shown numerous applications of the method for analyzing potential flow around a three-dimensional obstacle. The vorticity distribution on the obstacle surface was approximated by triangular surface elements, where each element has an assumed variation of vorticity. The number of equations in this case was equal to the number of boundary points on the obstacle surface at which the boundary condition for the normal velocity

$$u_n = 0 \tag{28}$$

was satisfied. This method is capable of treating arbitrarily-shaped obstacles and the number of unknowns was kept to a reasonable limit, since the determination of the entire velocity field around the obstacle was not necessary. A direct application of the method of representing the wing by a surface vorticity distribution can be applied to real flow problems. However, for an accurate representation of the wing geometry, the number of equations for the boundary conditions (three at each point on the surface) grows rapidly. Other applications of the method of singularities for determining the unsteady flow around a wing in the three-dimensional space exist in the literature.[15-17]

In this paper the method of singularities is applied in determining the velocity field around a wing in a more general manner.[18] The wing is represented by a system of point functions distributed inside the wing; each with a strength γ_i and position (x_i, y_i, z_i). These point functions can be point vortices, sources, or doublets, etc. The mathematical problem is then to determine $(\gamma_i, x_i, y_i, z_i)$ for n point sources that will represent the wing in the flowfield in the most accurate manner. If we define a variational functional

$$\Gamma = \int_S |\mathbf{u}|^2 \, dS \tag{29}$$

where S denotes the integration over the wing surface, the exact solution of the problem corresponds to

$$\Gamma(\gamma_i, x_i, y_i, z_i) = 0 \tag{30}$$

In Eq. (29), Γ is a positive, semi-definite nonlinear function of (x_i, y_i, z_i) and is linear with respect to γ_i. The velocity field around the wing can be expressed in terms of point vortices representing the wing and the surrounding vorticity field as

$$\mathbf{U} = -\frac{1}{4\pi}\left[\int_V \frac{\mathbf{r}' \times \mathbf{w}}{|\mathbf{r}'|^3} dV - \sum \frac{\gamma_i \mathbf{r}^*}{|\mathbf{r}^*|^3}\right] \tag{31}$$

where $\mathbf{r}^*$ is the relative position vector of a point in space with respect to a point vortex at (x_i, y_i, z_i) and $\mathbf{r}'$ with respect to another point with $\mathbf{w}$. Using Eq. (31), the functional Γ can be discretized at m points on the wing surface ($m \geqq n$) as

$$\bar{\Gamma} = \sum_m u_i{}^2 \Delta S_i \tag{32}$$

where ΔS represents the area of a finite surface element for which at the centroid $u_i = |\mathbf{u}|$. The discrete form of Eq. (31) can be written as

$$\mathbf{P}\gamma = \mathbf{C} \tag{33}$$

Vector $\mathbf{C}$ represents the induced velocity field at the surface of the wing due to the surrounding vorticity field. Then, Eq. (32) can be written as

$$\bar{\Gamma} = (\mathbf{P}\gamma - \mathbf{C})^t \mathbf{S}(\mathbf{P}\gamma - \mathbf{C}) \tag{34}$$

where $\mathbf{S}$ is a diagonal matrix with ΔS_i terms. The solution of Eq. (30) can be obtained by determining the optimum of $\mathbf{P}$ and γ. By minimizing $\bar{\Gamma}$ with respect to γ_i

$$\partial\bar{\Gamma}/\partial\gamma_i = 0 \tag{35}$$

one can obtain γ in terms of matrices $\mathbf{P}$, $\mathbf{S}$, and $\mathbf{C}$ as

$$\gamma = (\mathbf{P}^t\mathbf{S}\mathbf{P})^{-1}\mathbf{P}^t\mathbf{S}\mathbf{C} \tag{36}$$

Substituting into Eq. (34), Eq. (34) becomes

$$\bar{\Gamma} = \mathbf{C}^t\mathbf{S}\mathbf{C} - \mathbf{C}^t\mathbf{S}\mathbf{P}(\mathbf{P}^t\mathbf{S}\mathbf{P})^{-1}\mathbf{P}^t\mathbf{S}\mathbf{C} \tag{37}$$

Another parameter Ξ can be defined as

$$\Xi = \frac{\mathbf{C}^t\mathbf{S}\mathbf{P}(\mathbf{P}^t\mathbf{S}\mathbf{P})^{-1}\mathbf{P}^t\mathbf{S}\mathbf{C}}{\mathbf{C}^t\mathbf{S}\mathbf{C}} \tag{38}$$

where as $\bar{\Gamma} \to 0$, $\Xi \to 1$. It can also be shown that as $\Xi \to 1$, Ξ^* also goes to 1 where

$$\Xi^* = \frac{\mathbf{C}^t\mathbf{S}\mathbf{P}(\mathbf{P}^t\mathbf{S}\mathbf{P})\mathbf{P}^t\mathbf{S}\mathbf{C}}{(\mathbf{C}^t\mathbf{S}\mathbf{P}\mathbf{P}^t\mathbf{S}\mathbf{C})^2/(\mathbf{C}^t\mathbf{S}\mathbf{C})} \tag{39}$$

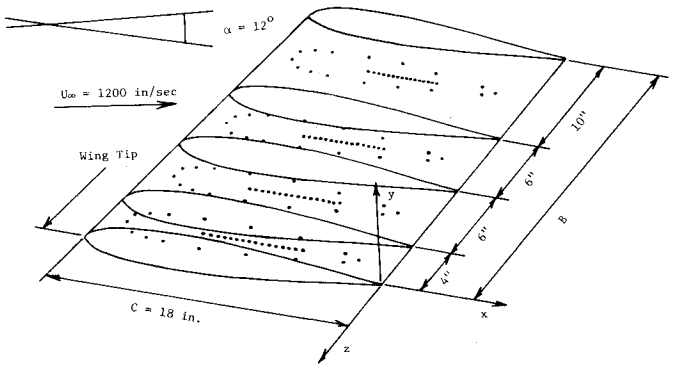

Fig. 3 Geometry of the wing in the analysis and the initial positions and directions of the doublets before the optimization process.

The problem is then to optimize Ξ^* by changing matrix **P**. In this case the optimization process does not require the inversion of a matrix as in the case of Eq. (38). The optimization process can be performed once at several time steps of the numerical integration, while the vector γ is determined at each step from Eq. (36). However, the product $\mathbf{P}'\mathbf{S}\mathbf{P}$ is inverted and stored only when the position of vortices are varied. Application of the procedure for a sample case is discussed in Sec. IV-B.

B. Representation of the Wing by a System of Vortices

Figure 3 shows the geometry of the wing used in this analysis.[19] It has a NACA 0012 airfoil cross section and is initially pitched at 12° angle of attack. In the analysis, the wing was represented by a series of point vortices along the chord and doublets closer to the surface as shown in Fig. 3. The streamlines around the wing, as obtained from this distribution of point vortices, are shown in Fig. 4. The variations of the velocities along the wing axis are shown in Fig. 5.

Certain modifications were made to decrease the computer time required for the optimization process based on physical correlations. The velocity field induced by each doublet was calculated only for points at the immediate neighborhood of each doublet. The streamlines corresponding to this version are quite similar to the ones in Fig. 6 of Ref. 20. Further experimentation was made by considering only the first three rows of doublets in Fig. 3. The results around the wing tip were still reasonable while the results degenerated at sections further along the spanwise direction.[20]

The positions of the doublets were then optimized by using the optimization technique described previously. The variation of Ξ^* with the number of iterations is discussed in Ref. 20. Accuracy of the results from the optimization routine was

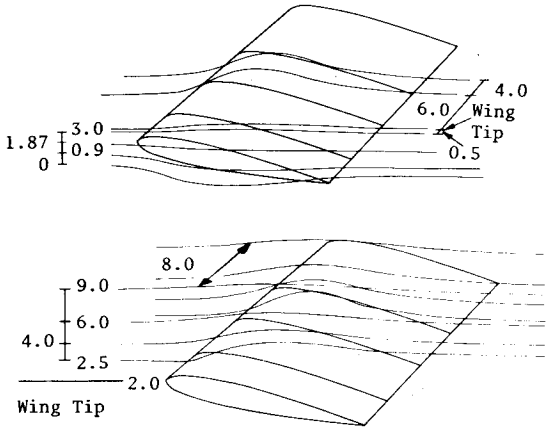

Fig. 4 Streamlines around the wing as calculated from the representation of the wing by the system of doublets.

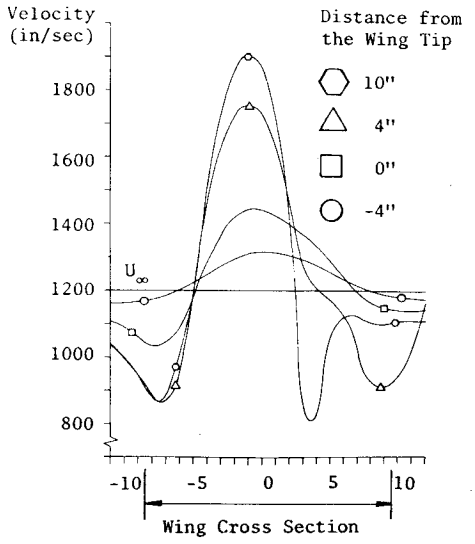

Fig. 5 Variation of velocities along streamlines at different cross sections of the wing. Negative distances means away from the wing tip. The streamlines start at the freestream at the same elevation of the wing tip.

analyzed by comparing the velocity distribution around the wing before and after the optimization. Again only the local effects of each source were considered. The comparison of the velocity field for two streamlines in Fig. 5 is shown in Fig. 6.

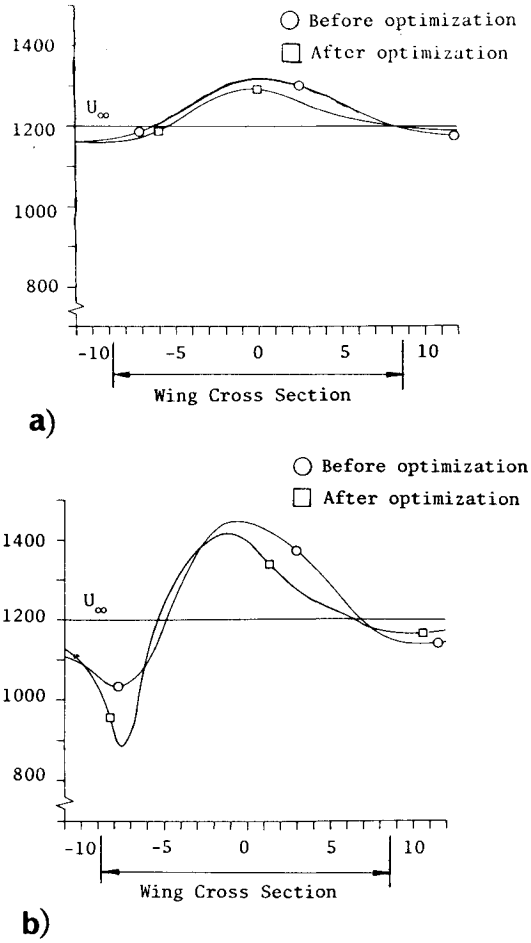

Fig. 6 Comparison of the variation of velocities along streamlines at the same cross sections of the wing as in Fig. 5 before and after the optimization process. a) −4 in. from the wing tip; b) 0 in. from the wing tip.

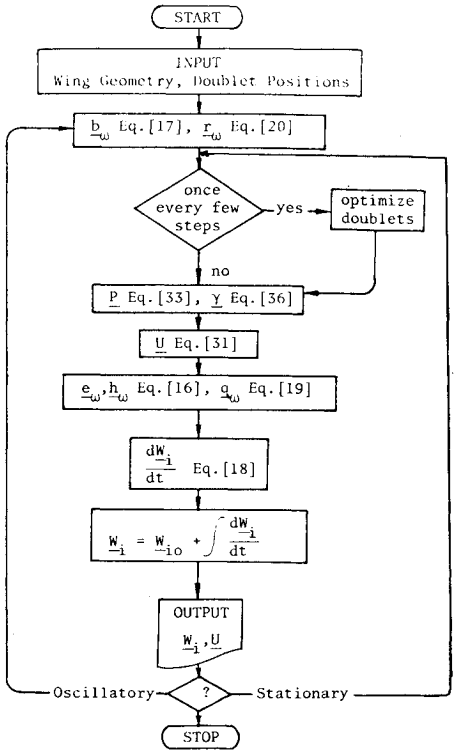

Fig. 7 Flow chart showing the over-all features of the computer program.

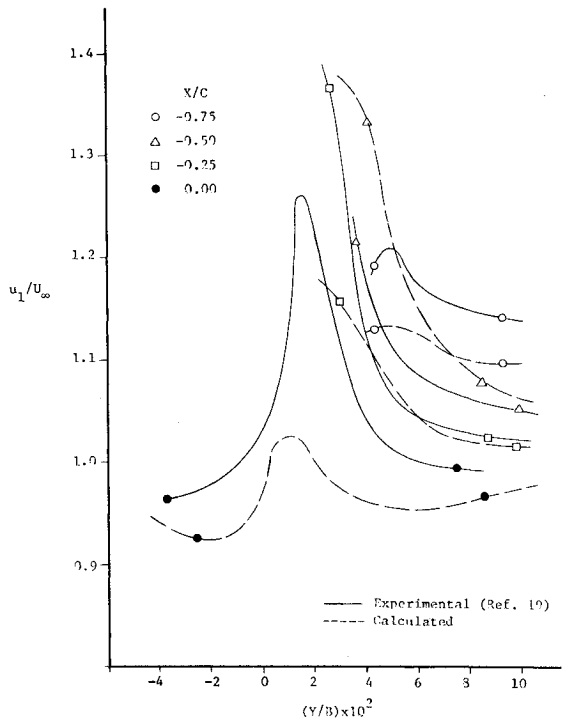

Fig. 8 Variation of chordwise velocities at the wing tip ($z = 0$) at different chordwise locations.

Summary of the Computational Procedure

The over-all computational procedure can be summarized as shown in the flow chart of Fig. 7. At each step of the numerical integration of the vorticity transport equations, the vorticity field is determined from Eq. (16). For an instantaneous velocity distribution, the vector **C** is calculated and the velocity field around the wing is determined at each node of the finite element gridwork shown in Fig. 1 from Eqs. (31) and (36). $d\mathbf{W}/dt$ is then calculated from Eq. (18) and integrated numerically.

At intermittent time steps of the numerical integration, the positions of point sources are optimized for a better representation of the wing geometry. In the case of the oscillating wing, matrix **P** was calculated at each time step of the integration; however, for stationary wing, it changed only after each optimization process.

Discussion

The analysis of unsteady flow around oscillating wings is of considerable practical importance. The suitability of the finite element method for the solution of the Navier-Stokes equations in three-dimensional space is demonstrated in this paper. Samples of the numerical results obtained from the described mathematical model are compared with the experimental results of Ref. 19. Velocity distributions along the wing chord were plotted following the streamlines, which started in the freestream at the same elevation as the leading edge of the pitched wing. The variations of the velocities in normal and chordwise directions are presented in Figs. 8–10. As can be seen in Fig. 8, at 0.50- and 0.75-chord length and at the trailing edge, the results for u_1 compared favorably with the experimental results. Similar behavior can be observed in comparing the velocities in the other two directions as shown in Figs. 9 and 10. However, at the 0.25-chord length, a flow separation indicated by the experimental results was not reproduced in Fig. 9. Figure 11 shows the wing-tip effect on the velocity distributions; variations of velocities are plotted along the spanwise direction at 0.75-chord length locations. As can be seen the three-dimensional flow effects around the wing-tip become more pronounced close to the wing.

The wing was then oscillated around its 0.25-chord length axis by $\omega = 50$ cps. Such numerical results are illustrated in Fig. 12 and compared with the results at the same angle of attack for a stationary wing. The changes in the velocity field due to oscillation are shown at 0.50-chord length and at the trailing edge of the wing chord.

This paper contains a direct formulation of the finite element method for the Navier-Stokes equations, which was applied by the authors in an effort to extend a previous analysis.[6] A major concern in this application was the need of a direct

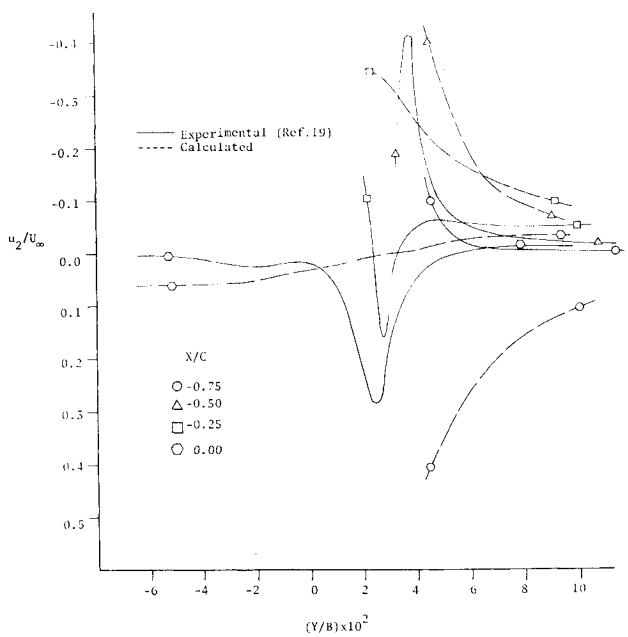

Fig. 9 Variation of normal velocities at the wing tip ($z = 0$) at different chordwise locations.

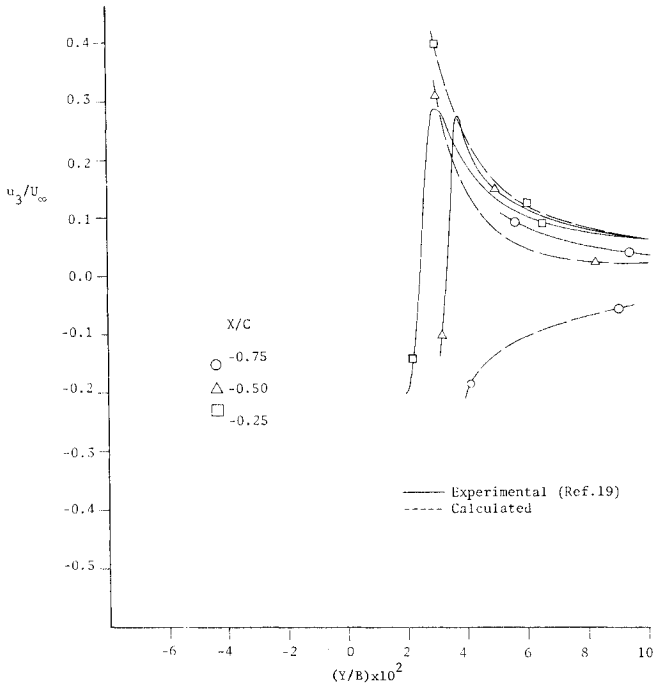

Fig. 10 Variation of spanwise velocities at the wing tip ($z = 0$) at different chordwise locations.

specification of the wing boundary conditions at a series of points on the wing boundary, which becomes uneconomical with increasing number of points. An accurate determination of the three-dimensional velocity field is required for the numerical integration of the vorticity transport equations. Obtained results show that the method of singularities can be employed for an efficient determination of the velocity field. Decisions have to be made in terms of the number of point vortices, necessary number of points on the wing boundary for adequate representation of the wing, and initial assumption of positions of the point vortices. The applied optimization procedure generalizes the method and gives a measure of accuracy of results in terms of Ξ^*.

The computer storage requirement depends basically on the size of matrix **b**; its size defined by the number of points on the wing boundary times the number of total grid points. The simplification of matrix **b**, as in the case of matrix $\mathbf{r}_\omega$ reduces the required storage significantly. Computer time depends

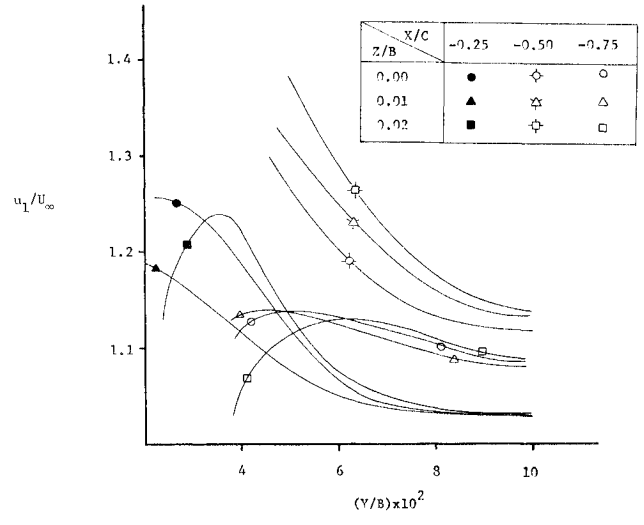

Fig. 11 Variation of chordwise velocities at different points on the wing chord at different spanwise sections.

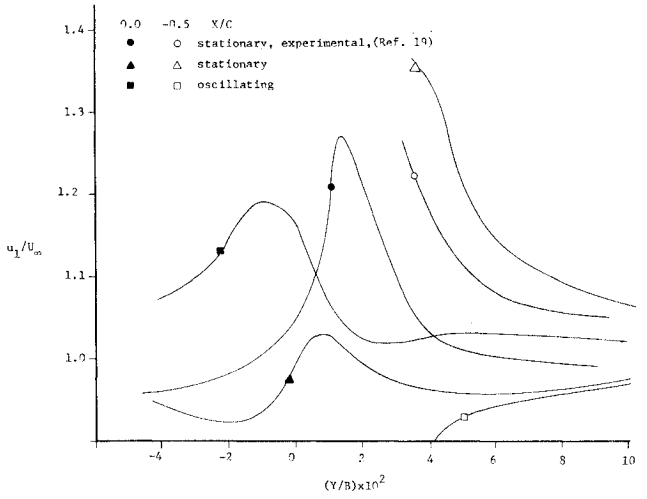

Fig. 12 Comparison of chordwise velocities at two points on the wing chord when the wing is stationary and pitching ($\omega = 50$ cps) at $\alpha = 12°$.

strongly on the calculation of the velocity field because of the system of doublets representing the wing and the surrounding vorticity field. The described computational procedure for determining the velocity field reduces the required computer time considerably. Numerical errors resulting from discretization of the vorticity transport equations can be considered in terms of the over-all accuracy of the numerical integration procedure. The accuracy and stability problems in the solution of Navier-Stokes equations can be handled efficiently using the finite element method as discussed in Ref. 7.

Appendix A : Derivation of the Vector $\mathbf{h}_{\omega i}$

From Eqs. (9) and (16) the vector $\mathbf{h}_\omega$ can be obtained from the optimization of the following variational functional:

$$\Phi^* = \frac{1}{2}\int_V \omega_i u_j \frac{\partial \omega_i}{\partial x_j} dV + \frac{\nu}{2}\int_V \left(\frac{\partial \omega_i}{\partial x_j}\right)^2 dV - \frac{1}{2}\int_V \omega_i \omega_j \frac{\partial u_i}{\partial x_j} dV \tag{A1}$$

By discretizing Φ^* using Eq. (7) and minimizing with respect to W_i^j, $\mathbf{h}_{\omega i}$ can be obtained as

$$\partial \Phi^* / \partial W_i^j = \mathbf{h}_{\omega i}{}^j \tag{A2}$$

from which

$$\mathbf{h}_i = \left\{\sum_g \int_V [\mathbf{A}^t\mathbf{A}\mathbf{P}\mathbf{A}_x + \mathbf{A}^t\mathbf{A}\mathbf{q}\mathbf{A}_y + \mathbf{A}^t\mathbf{A}\mathbf{w}\mathbf{A}_z]\, dV + \sum_g \int_V \nu[\mathbf{A}_x{}^t\mathbf{A}_x + \mathbf{A}_y{}^t\mathbf{A}_y + \mathbf{A}_z{}^t\mathbf{A}_z]\, dV\right\}\mathbf{W}_i + \mathbf{T}_d{}^i(\mathbf{W}_k) \tag{A3}$$

For $\mathbf{W}_1$

$$T_d{}^1(W_k) = \sum_g \int_V \mathbf{A}^t(\mathbf{A}_x \mathbf{p}\mathbf{A}\mathbf{W}_1 + \mathbf{A}_y \mathbf{p}\mathbf{A}\mathbf{W}_2 + \mathbf{A}_z \mathbf{p}\mathbf{A}\mathbf{W}_3)\, dV \tag{A4}$$

From Eqs. (A3) and (A4), $\mathbf{h}_{\omega i}$ can be written as

$$\mathbf{h}_{\omega i} = [\mathbf{D}_{c1} + \mathbf{D}_{c2} + \mathbf{D}_{c3}]\mathbf{W}_i + \nu \mathbf{D}_\nu \mathbf{W}_i + \mathbf{T}_d{}^i(W_k) \tag{A5}$$

where

$$\mathbf{T}_d{}^i(\mathbf{W}_k) = \mathbf{E}_1{}^i\mathbf{W}_1 + \mathbf{E}_2{}^i\mathbf{W}_2 + \mathbf{E}_3{}^i\mathbf{W}_3 \tag{A6}$$

Details of each of the matrices in Eqs. (A3–A6) are given in Ref. 20.

References

[1] Fromm, J. E., "A Method for Computing Nonsteady, Incompressible, Viscous Fluid Flows," Rept. LA-2910, Sept. 1963, Los Alamos Scientific Lab., Los Alamos, N. Mex.

[2] Thoman, D. C. and Szewczyk, A. A., "Time-Dependent Viscous Flow over a Circular Cylinder," *Physics of Fluids Supplement*, Vol. 12, No. 12, Dec. 1969, p. 76.

[3] Cheng, S. J. and Rimon, Y., "Numerical Solution of a Uniform Flow Over a Sphere at Intermediate Reynolds Numbers," *Physics of Fluids*, Vol. 12, No. 5, May 1969, p. 949.

[4] Rimon, Y., "Numerical Solution of the Incompressible Time-Dependent Viscous Flow past a Thin Oblate Spheroid," *Physics of Fluids Supplement*, Vol. 12, No. 12, Dec. 1969, p. 65.

[5] Thompson, J. F. F. Jr., Shanks, S. P., and Wu, J. C., "Numerical Solution of the Three-Dimensional Navier-Stokes Equations showing Trailing Tip Vortices," *AIAA Journal*, Vol. 12, No. 6, June 1974, pp. 787–794.

[6] Bratanow, T., Ecer, A., and Kobiske, M., "Finite Element Analysis of Unsteady Incompressible Flow Around an Oscillating Obstacle of Arbitrary Shape," *AIAA Journal*, Vol. 11, No. 11, Nov. 1973, pp. 1471–1477.

[7] Bratanow, T. and Ecer, A., "On the Application of the Finite Element Method in Unsteady Aerodynamics," *AIAA Journal*, Vol. 12, No. 4, April 1974, pp. 503–510.

[8] Bratanow, T., Ecer, A., and Kobiske, M., "Numerical Calculations of Velocity and Pressure Distribution Around Oscillating Airfoils," CR-2368, March 1974, NASA.

[9] Cheng, R. T. S., "Numerical Solution of the Navier-Stokes Equations by the Finite Element Method," *Physics of Fluids*, Vol. 15, No. 12, 1972, pp. 2093–2105.

[10] Taylor, C. and Hood, P., "A Numerical Solution of the Navier-Stokes Equations Using the Finite Element Technique," *International Journal of Computer and Fluids*, Vol. 1, No. 1, 1973, pp. 73–100.

[11] Bratanow, T. and Ecer, A., "Analysis of Moving Body Problems in Aerodynamics," *Finite Element Methods in Flow Problem, Collected Papers from the International Symposium at the University of Wales*, edited by J. F. Oden, O. C. Zienkiewics, R. H. Gallagher, and C. Taylor, Univ. of Wales, Swansea, Wales, 1974, pp. 225–241.

[12] Bratanow, T. and Ecer, A., "Suitability of the Finite Method for Analysis of Unsteady Flow Around Oscillating Airfoils," International Conference on Numerical Methods in Fluid Dynamics, Univ. of Southampton, Southampton, England, Sept. 26–28, 1973.

[13] Prager, W., "Die Druckverteilung an Koerpern in ebener Potentialstroemung," *Zeitschrift für Physik*, Vol. XXIX, 1928, pp. 865–869.

[14] Hess, K. L. and Smith, A. M. O., "Calculation of Potential Flow About Arbitrary Bodies," *Progress in Aerospace Sciences*, Vol. 8, edited by D. Kuchemann, Pergamon Press, New York, 1967, pp. 1–138.

[15] Kress, R., "Treatment of the Prager Problem of Potential Theory by the Integral Equation Method," *Physics of Fluids*, Vol. 12, No. 12, Dec. 1969, p. 120.

[16] Botta, E. F. F. and van de Vooren, A. I., "Calculation of Potential Flow about Aerofoils Using Approximation by Splines," *Contributions to the Theory of Aircraft Structures*, Delft University Press, Delft, The Netherlands, 1972.

[17] Argyris, J. H. and Scharpf, D. W., "Two- and Three-Dimensional Potential Flow by the Method of Singularities," *Journal of the Royal Aeronautical Society*, Vol. 73, 1969, pp. 959–961.

[18] Ecer, A., "Application of the Method of Singularities in the Analysis of Brittle Fracture," *Proceedings of the 10th Anniversary Meeting of the Society of Engineering Sciences*, North Carolina State Univ., Raleigh, N.C., Nov. 1973, to be published.

[19] Chigier, H. A. and Corsiglia, V. R., "Tip Vortices-Velocity Distributions," Preprint 522, 27th Annual Nat. V/STOL Forum of the American Helicopter Soc., Washington, D.C., May 1971.

[20] Bratanow, T. and Ecer, A., "Analysis of Three-Dimensional Unsteady Flow Around Oscillating Wings," AIAA Paper 74-184, Washington, D.C., 1974.